Article

Single-atom Fe Embedded Co_3S_4 for Efficient Electrocatalytic Oxygen Evolution Reaction

QI Yuxue[1#], LI Tingting[1#], HU Yajie[1#], XIANG Jiahong[1], SHAO Wenqian[1], CHEN Wenhua[2], MU Xueqin[3], LIU Suli[1], CHEN Changyun[1], YU Min[1]✉ and MU Shichun[3]✉

Received July 21, 2022
Accepted August 28, 2022

Constructing atomically dispersed active sites with densely exposed and dispersed double metal-S_x catalytic sites for favorable OER catalytic activity remains rare and challenging. Herein, we design and construct a $Fe_1S_x@Co_3S_4$ electrocatalyst with Fe single atoms epitaxially confined in Co_3S_4 nanosheets for catalyzing the sluggish alkaline oxygen evolution reaction(OER). Consequently, in ultralow concentration alkaline solutions(0.1 mol/L KOH), such a catalyst is highly active and robust for OER with low overpotentials of 300 and 333 mV at current densities of 10 and 30 mA/cm^2, respectively, accompanying long-term stability without significant degradation even for 350 h. In addition, $Fe_1S_x@Co_3S_4$ shows a turnover frequency(TOF) value of 0.18 s^{-1}, nearly three times that of Co_3S_4(0.07 s^{-1}), suggesting the higher atomic utilization of Fe single atoms. Mössbauer and *in-situ* Raman spectra confirm that the OER activity of $Fe_1S_x@Co_3S_4$ origins from a thin catalytic layer of Co(Fe)OOH that interacts with trace-level Fe species in the electrolyte, creating dynamically stable active sites. Combined with experimental characterizations, it suggests that the most active S-coordinated dual-metal site configurations are 2S-bridged (Fe-Co)S_4, in which Co-S and Fe-S moieties are shared with two S atoms, which can strongly regulate the adsorption energy of reaction intermediates, accelerating the OER reaction kinetics.

Keywords Electrocatalyst; Dual-metal site; S coordination; Fe single atom; Oxygen evolution reaction

1 Introduction

Oxygen evolution reaction(OER) is the rate-determining step for water electrolysis owing to the multistep electron transfer process, leading to slow kinetics and restricting the large-scale application of hydrogen production from water electrolysis[1,2]. In this context, IrO_2 and RuO_2 as benchmarks have high OER catalysis capability, but their high cost and scarcity significantly impede industrial applications[3,4]. Thus, it is urgent to develop more advanced and inexpensive catalysts with high activity and stability to promote the development of next-generation energy utilization technologies.

Cobalt sulfides are promising catalysts in alkaline OER due to their cost-effectivity and large-scale manufacturing capability[5,6]. However, their OER activity and stability are still far from being satisfactory for meeting commercial applications[7,8]. Further modifications, such as doping, strain, and defect engineering can effectively tailor the adsorption-free energy of oxygen-involved intermediate species and conduct OER in lower energy barriers[9−11]. Recent studies showed that Co_3S_4 can exhibit great potential as ideal support to stabilize the single atom by metal coupling sulfide(M-S_x), maximizing the catalytic activity of active sites by modulating the local atomic configuration and electronic structure, and leading to dramatically improved OER performance[11,12]. More interestingly, the incorporation of Fe atoms would effectively improve the electrocatalytic performance of catalysts, profiting from the favorable change of O and OH adsorption energy on the Co sites[13,14].

In addition, Fe introduction could boost the electron-transfer rate and induce the formation of defect sites due to different valence states[15]. Therefore, such a facile strategy can be employed to prepare highly active single atom catalysts with metal coupling sulfide(M-S_x).

Herein, Co_3S_4 nanosheets with rich defects are selected as an ideal support to fabricate Fe single-atom catalysts to enhance the OER activity. In detail, in an ultralow concentration solution of 0.1 mol/L KOH, $Fe_1S_x@Co_3S_4$ reaches low overpotentials with excellent stability maintained within 350 h. Combined with *in-situ* Raman spectroscopy and electrochemical tests, it can be concluded that the presence of the 2S-bridged(Fe-Co)S_4 coordination configuration as a new active site significantly enhances the OER activity of $Fe_1S_x@Co_3S_4$. Moreover, benefiting from S coordination of a dual-metal site process, it can achieve much more accessibility to atomically isolated catalytic sites, favorable for the adjustable electronic structure of the active centers, and thus influencing the electrocatalytic performance.

✉ YU Min
minyu@nuaa.edu.cn
✉ MU Shichun
msc@whut.edu.cn
#These authors contributed equally to this work.
1. Key Laboratory of Advanced Functional Materials of Nanjing, Nanjing Xiaozhuang University, Nanjing 211171, P. R. China;
2. Co-Innovation Center of Efficient Processing and Utilization of Forest Resources, College of Materials Science and Engineering, Nanjing Forestry University, Nanjing 210037, P. R. China;
3. State Key Laboratory of Advanced Technology for Materials Synthesis and Processing, Wuhan University of Technology, Wuhan 430070, P. R. China

https://doi.org/10.1007/s40242-022-2248-x

2 Experimental

The experiment section and characterization can be seen in the Electronic Supplementary Material of this paper.

3 Results and Discussion

The atomically dispersed $Fe_1S_x@Co_3S_4$ catalysts were obtained in two consecutive steps. Briefly, $Fe(NH_4)_2{\cdot}(SO_4)_2{\cdot}6H_2O$ and Co-MOF were dispersed in a mixture of 1-dodecanethiol(DT), and dodecylamine(DDA), and stirred vigorously at room temperature. Subsequently, Co(Fe)-MOF was converted into $Fe_1S_x@Co_3S_4$ through a solid-liquid phase chemical route. Transmission electron microscopy(TEM) images show that $Fe_1S_x@Co_3S_4$ has an ultrathin nanosheet structure[Figs.1(A) and Fig.S1, see the Electronic Supplementary Material of this paper]. Notably, the aberration-corrected high-resolution TEM(HRTEM) image(Fig.S2, see the Electronic Supplementary Material of this paper) further discloses that the rough surface of nanosheets is composed of disordered lattice structures, which facilitates the electron transfer, beneficial for improving the OER activity[16,17]. The *d*-spacing (111) of $Fe_1S_x@Co_3S_4$ obviously increases after the addition of Fe[Figs.1(B) and Fig.S3, see the Electronic Supplementary Material of this paper], meanwhile, the electron energy loss spectroscopy (EELS) spectrum further identified the embedding of Fe sites within the atomic Co_3S_4 lattice[Figs.1(C) and Fig.S4, see the Electronic Supplementary Material of this paper][18]. Notably, as shown in Fig.1(D) and (E), single Fe atoms are distinguished and anchored on the surface of the Co_3S_4 matrix. The atomic dispersion of Fe species in $Fe_1S_x@Co_3S_4$ is further confirmed by the analysis of intensity profiles[Fig.1(E)][19], in which Fe, S, and Co elements are uniformly distributed on the $Fe_1S_x@Co_3S_4$ surface[Fig.1(F)]. And the Fe content was measured to be 6.59%(mass fraction) by inductively coupled plasma-atomic emission spectrometry(ICP-AES) measurement(Table S1, see the Electronic Supplementary Material of this paper).

Powder X-ray diffraction(XRD) patterns show that the diffraction peaks of Co_3S_4 coincide well with that of the standard cubic Co_3S_4(JCPDS No. 42-1448), suggesting the Fe introduction did not alter the main structure of Co_3S_4 and no crystalline Fe formed[Fig.2(A)]. Also, upon the addition of Fe, the dominant peaks gradually shift toward lower diffraction angles, which testifies to the successful incorporation of Fe species[20]. The formation of $Fe_1S_x@Co_3S_4$ was further confirmed by Raman spectrum spectroscopy[Fig.2(B)]. The typical characteristic vibrations are attributed to vibrational modes of the Co—S bond and that at 658.5 cm^{-1} is due to the S—S stretching vibration, verifying the formation of separated CoS_x species(Table S2, see the Electronic Supplementary Material of this paper)[21]. Notably, the E_g peak obviously broadens and undergoes blue shifts arising from the Fe atoms doping in the Co_3S_4 lattice and increased short-range disorder of $Fe_1S_x@Co_3S_4$ crystals(Fig.S5, see the Electronic Supplementary Material of this paper)[22,23].

Furthermore, according to the XPS spectra, the presence of Co, Fe, and S elements in the $Fe_1S_x@Co_3S_4$ catalyst can be

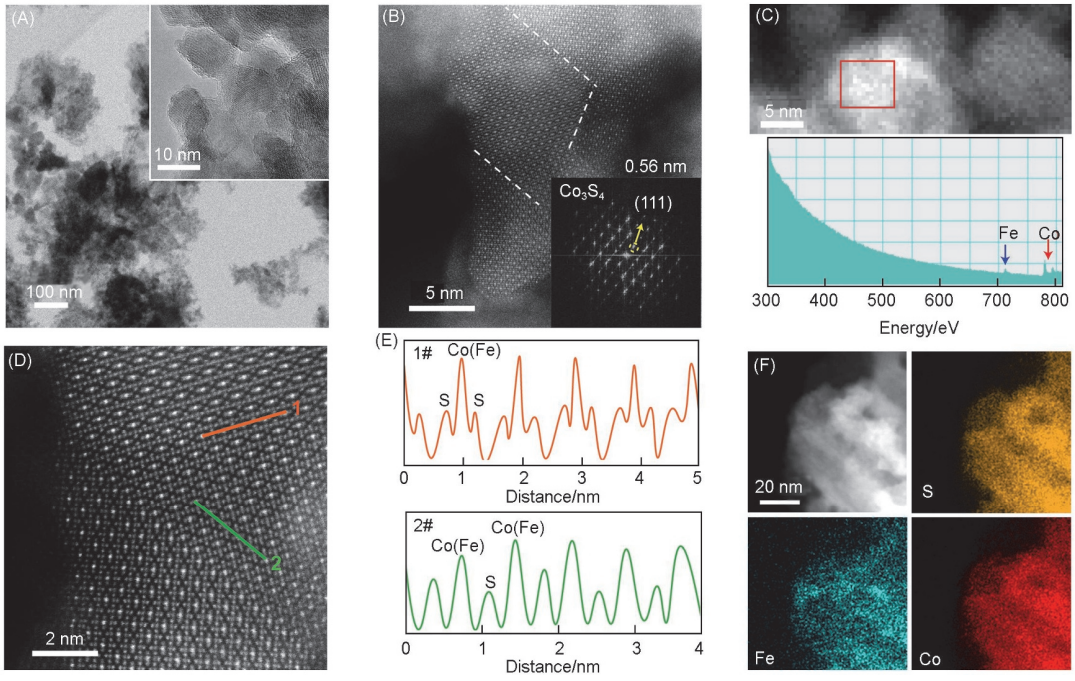

Fig.1 TEM images(the inset is an enlarged TEM view showing the structure of the nanosheets)(A), HRTEM image(B), HAADF-STEM image and corresponding EELS spectrum(C), intensity profiles of $Fe_1S_x@Co_3S_4$ obtained in the dotted rectangle regions 1# and 2# in (D)(D, E) and HAADF-STEM and corresponding elemental mapping images of $Fe_1S_x@Co_3S_4$(F)

https://doi.org/10.1007/s40242-022-2248-x

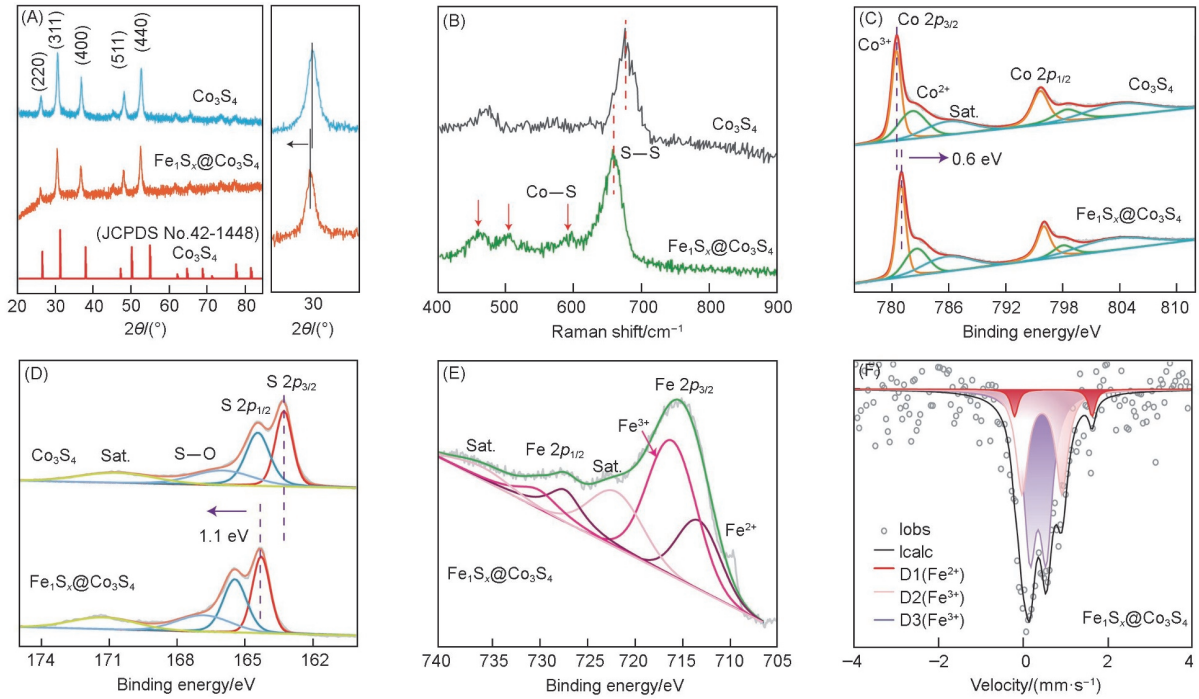

Fig.2 XRD patterns(A) and Raman spectra(B) of $Fe_1S_x@Co_3S_4$ and Co_3S_4, respectively, Co 2*p*(C), S 2*p*(D), Fe 2*p*(E) regions of $Fe_1S_x@Co_3S_4$ and Co_3S_4, respectively, and ^{57}Fe Mössbauer spectra of $Fe_1S_x@Co_3S_4$(F)

verified(Fig.S6, see the Electronic Supplementary Material of this paper). In Fig.2(C), the emerged peaks at 780.5 and 795.7, and 782.3 and 798.6 eV correspond to the Co^{3+} and Co^{2+}, respectively[24]. The binding energy increases by 0.6 eV for $Fe_1S_x@Co_3S_4$, which reflects the Co loses electrons after the Fe introduction. And the doublet peaks located at 163.3 and 164.4 eV in the high-resolution S 2*p* spectrum of $Fe_1S_x@Co_3S_4$ [Fig.2(D)] are attributed to the formation of metal-S chemical bonds[25]. Moreover, the incorporation of Fe single-atom into the lattice may lead to the blue shift of the binding energy. Additionally, the characteristic peaks at 713.3 and 716.2 eV in the spectra of $Fe_1S_x@Co_3S_4$ can be attributed to Fe^{2+} and Fe^{3+}, respectively[Fig.2(E)][26]. Further structural insights about the Fe species in $Fe_1S_x@Co_3S_4$ were performed in terms of the Mössbauer spectrum[27]. As shown in Fig.2(F) and Table S3(see the Electronic Supplementary Material of this paper), the fitting result of the $Fe_1S_x@Co_3S_4$ indicates the existence of both Fe^{2+} and Fe^{3+}. Taken together, these measurement results indicate that the atomic Fe_1S_x units can be confined in Co_3S_4, which plays a significant role in the regulation of the electrocatalytic activity.

The electrocatalytic performance of Co-MOF, commercial RuO_2, commercial IrO_2, $Fe_1S_x@Co_3S_4$, and Co_3S_4(Fig.S7, see the Electronic Supplementary Material of this paper) toward the OER was tested in a 0.1 mol/L KOH aqueous solution[28,29]. As shown in Fig.3(A), $Fe_1S_x@Co_3S_4$ delivers an OER current density of 10 mA/cm² at an overpotential of 300 mV, which is 21 and 82 mV lower than that of Co_3S_4 and IrO_2, respectively. Further, to generate 30 mA/cm², $Fe_1S_x@Co_3S_4$ presents a smaller overpotential of 333 mV, while Co_3S_4, commercial RuO_2, and commercial IrO_2 required 357, 355, and 452 mV, respectively [Fig.3(A), Table S4, see the Electronic Supplementary Material of this paper]. Thus, it is clear that Fe doping can effectively improve OER performance. The corresponding Tafel slope for $Fe_1S_x@Co_3S_4$ was fitted to be 59 mV/dec, revealing favorable OER kinetics[Fig.3(B)][30]. Strikingly, it even presents performance advantages when compared with the other samples and the state-of-art OER electrocatalysts as reported in the same KOH solutions[Fig.3(C) and Table S5, see the Electronic Supplementary Material of this paper].

To understand the origin of the high OER activity of $Fe_1S_x@Co_3S_4$, the C_{dl} was used to evaluate the electrochemically active surface areas(ECSAs) of catalysts[31]. The C_{dl} values of $Fe_1S_x@Co_3S_4$(105 mF/cm²), Co_3S_4(35 mF/cm²), and Co-MOF(38 mF/cm²) are shown in Fig.3(D) and Fig.S8(see the Electronic Supplementary Material of this paper), in which $Fe_1S_x@Co_3S_4$ has a larger C_{dl} and thus a higher ECSA compared to other catalysts. In other words, the optimal Fe incorporation is beneficial for increasing the number of catalytically active sites, thus making a great contribution to the OER performance. Moreover, from Fig.3(E), $Fe_1S_x@Co_3S_4$ possesses a smaller R_{CT} value(29.7 Ω) than Co_3S_4(77.6 Ω) and Co-MOF(178 Ω), demonstrating that the Fe single-atom doping does accelerate the reaction kinetics(the fitting curves are presented in Fig.S9, see the Electronic Supplementary Material of this paper)[8]. Note that, as shown in Fig.3(F), the turnover frequency(TOF)

https://doi.org/10.1007/s40242-022-2248-x

value of catalysts was calculated at an overpotential of 50 mV, in which $Fe_1S_x@Co_3S_4$ shows a TOF value of 0.18 s^{-1}, nearly three times that of Co_3S_4(0.07 s^{-1}), suggesting the higher atomic utilization of Fe single-atom in $Fe_1S_x@Co_3S_4$. Further, the long-term stability of $Fe_1S_x@Co_3S_4$ was measured at a overpotential of 300 mV, without significant degradation after the 350 h test[Fig.3(G)], further attesting its superior long-term stability for OER.

To identify the activation process of the $Fe_1S_x@Co_3S_4$ electrode during the OER process, the corresponding *in situ* Raman spectrum was carried out[32]. As shown in Fig.4(A), the peaks at 446 and 614 cm^{-1} are attributed to E_g and A_g modes of CoO_2[Fig.4(B)][33]. With the increasing potential, the characteristic band of CoOOH overlaps with the Co—O, vibration at 446 cm^{-1}. Then, the surface reconstruction of the Co species was investigated by continuous cyclic voltammetry (CV) cycles[Fig.4(C)], consistent with the analysis results of *in-situ* Raman spectra and the previous reports[34]. Furthermore

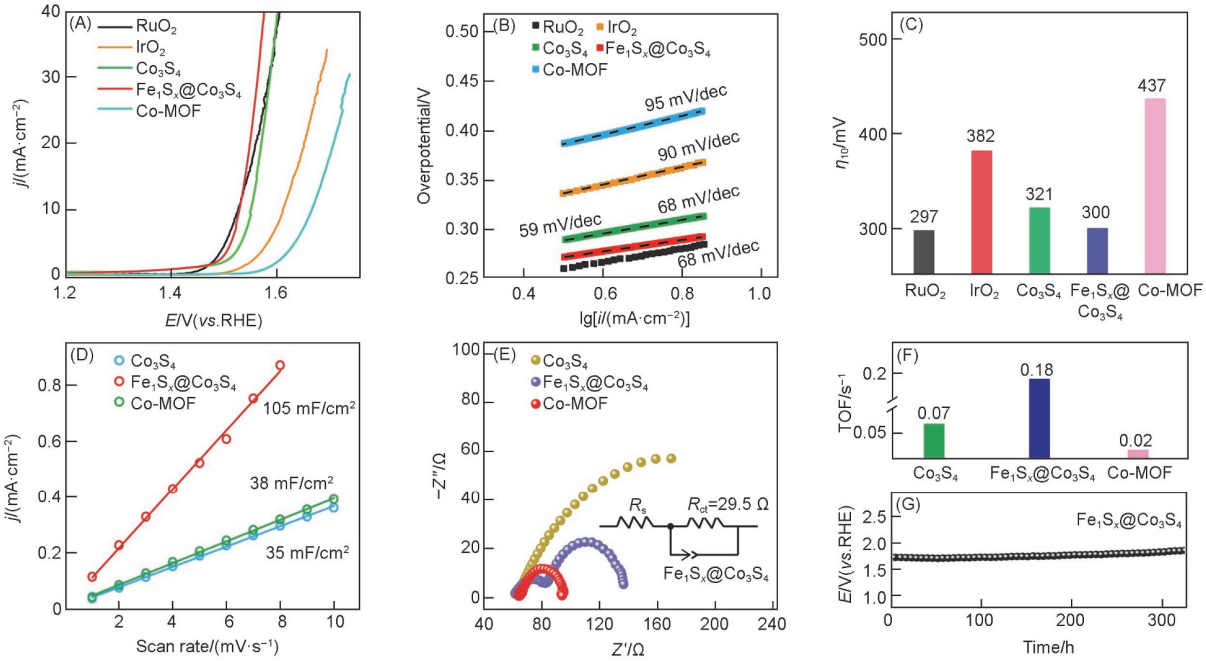

Fig.3 LSV curves(A), corresponding Tafel slopes(B), intrinsic activity(C), C_{dl} values(D), Nyquist plots(E), TOF curves(F) of catalysts, and the stability of $Fe_1S_x@Co_3S_4$(G)

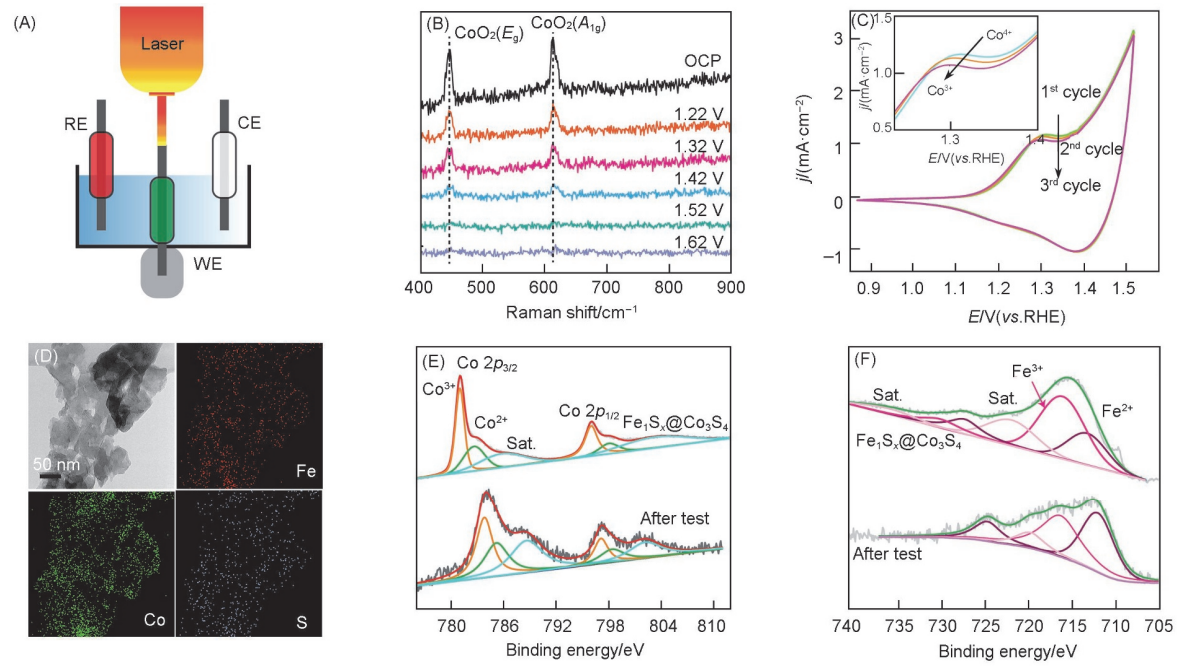

Fig.4 *In situ* electrochemical Raman cell set-up(A), *in situ* Raman spectra of $Fe_1S_x@Co_3S_4$ at different applied potentials(B), cyclic voltammetry of $Fe_1S_x@Co_3S_4$ with a 5 mV/s scan rate from 0.85 V to 1.50 V_{RHE}(C), elemental mapping images(D), Co 2*p* XPS(E), and Fe 2*p* XPS(F) spectra of $Fe_1S_x@Co_3S_4$ after stability test

https://doi.org/10.1007/s40242-022-2248-x

a low level of Fe substitution could facilitate surface reconstruction of inactive Co3S4 with the self-termination ability by activating the pre-oxidation of Co and introducing greater structural flexibility *via* uplifting the O 2*p* level of oxide[35]. Simultaneously, *in situ* doping of Fe during the synthesis process can ensure $Fe_1S_x@Co_3S_4$ with much more stable$(Fe\text{-}Co)S_4$ sites to offer improved catalytic and structural stability[35]. Meanwhile, to further provide the role of surface single atoms on water dissociation kinetics, TEM and XPS analyses were performed. As can be seen in Fig.4(D), the nanosheet structure of $Fe_1S_x@Co_3S_4$ remains. Similarly, the XPS results show that the peak positions of Co, and Fe do not change[Fig.4(E) and (F)], confirming the excellent stability during the OER process. However, the peak area of Co^{3+} in the Co 2*p* XPS spectrum of $Fe_1S_x@Co_3S_4$ increases, indicating the formation of metal hydroxides, which is accorded with the above *in situ* characterizations.

4 Conclusions

In summary, we reported the atomically dispersed Fe-S_x site embedded in Co_3S_4 nanosheets(devoted as $Fe_1S_x@Co_3S_4$) as a highly efficient catalyst for OER. Both Mössbauer and *in situ* Raman analyses revealed that the isolated metal single atom significantly enhanced the OER catalytic activity, due to the formation of most active S-coordinated dual-metal site configurations with 2S-bridged $(Fe\text{-}Co)S_4$ sites. The experimental test showed that $Fe_1S_x@Co_3S_4$ had excellent activity and stability toward OER with negligible activity decay within 350 h in a 0.1 mol/L KOH solution. This work offers new fundamental insights into the reaction kinetics and the state of the atomically dispersed centers under reactive conditions, which possesses broad application prospects.

Electronic Supplementary Material

Supplementary material is available in the online version of this article at http://dx.doi.org/10.1007/s40242-022-2248-x.

Acknowledgements

This work was supported by the National Natural Science Foundation of China (Nos.21501096, 22075223), the Natural Science Foundation of Jiangsu Province, China(Nos.BK20150086, BK20201120), the Foundation of the Jiangsu Education Committee, China(No.15KJB150020), the Six Talent Peaks Project in Jiangsu Province, China(No.JY-087), the Innovation Project of Jiangsu Province, Excellent Scientific and Technological Innovation Team of Colleges and Universities of Jiangsu Province, China(No.SUJIAOKE 2021 No.1), the Key Subject of Ecology of Jiangsu Province, China(No.SUJIAOYANHAN 2022 No.2), and the Project of the Scientific and Technological Innovation Team of Nanjing, China(No.NINGJIAOGAOSHI 2021 No.16).

Conflicts of Interest

The authors declare no conflicts of interest.

References

[1] Li X. L., Lei H. T., Xie L. S., Wang N., Zhang W., Cao R., *Acc. Chem. Res.*, **2022**, *55*(6), 878

[2] Yuan S., Peng J. Y., Cai B., Huang Z. H., Garcia-Esparza A. T., Sokaras D., Zhang Y. R., Giordano L., Akkiraju K., Zhu Y. G., Hübner R., Zou X. D., Román-Leshkov Y., Shao-Horn Y., *Nat. Mater.,* **2022**, *21*, 673

[3] Grimaud A., Diaz-Morales O., Han B. H., Hong W. T., Lee Y. L., Giordano L., Stoerzinger K. A., Koper M. T. M., Shao-Horn Y., *Nat. Chem.,* **2017**, *9*, 457

[4] Lei J., Zeng M. Q., Fu L., *Chem. Res. Chinese Universities,* **2020**, *36*(4), 504

[5] Thangasamy P., Oh S., Nam S., Randriamahazaka H., Oh I., *Small*, **2020**, *16*(6), 2001665

[6] Liu S. L., Che C. J., Jing H. Y., Zhao J., Mu X. Q., Zhang S. D., Chen C. Y., Mu S. C., *Nanoscale*, **2020**, *12*, 3129

[7] Yang J., Zhu G. X., Liu Y. J., Xia J. X., Ji Z. Y., Shen X. P., Wu S. K., *Adv. Funct. Mater.,* **2016**, *12*(26), 4712

[8] Zhou Y. X., Luo M., Zhang Z. C., Li W. R., Shen X. S., Xia W. W., Zhou M., Zeng X. H., *Appl. Surf. Sci.*, **2018**, *454*(1), 46

[9] Ji Q. Q., Kong Y., Tan H., Duan H. I., Li N., Tang B., Wang Y., Feng S. H., Lv L. Y., Wang C., Hu F. C., Zhang W. H., Cai L., Yan W. S., *ACS Catal.*, **2022**, *12*(8), 4318

[10] Sun T., Zang W. J., Yan H., Li J., Zhang Z. Q., Bu Y. F., Chen W., Wang J., Lu J., Su C. L., *ACS Catal.,* **2021**, *11*(8), 4498

[11] Li X. M., Zheng K. T., Zhang J. J., Li G. N., Xu C. J., *ACS Omega*, **2022**, *7*(14), 12430

[12] Zhu X. J., Dai J. L., Li L. G., Zhao D. K., Wu Z. X., Tang Z. H., Ma L. J., Chen S. W., *Carbon*, **2020**, *160*(30), 133

[13] Smith R. D. L., Prévot M. S., Fagan R. D., Trudel S., Berlinguette C. P., *J. Am. Chem. Soc.,* **2013**, *135*(81), 11580

[14] Zhang S., Huang B. L., Wang L. G., Zhang X. Y., Zhu H. S., Zhu X. Q., Li J., Guo S. J., Wang E., *ACS Appl. Mater. Interfaces,* **2020**, *12*(36), 40220

[15] Wei P. K., Yang Y., Kang H. Z., Hao Z. W., Guo D. G., Liu L., *Chem. Eur. J.*, **2020**, *26*(60), 13725

[16] Xu L., Jiang Q. Q., Xiao Z. H., Li X. Y., Huo J., Wang S. Y., Dai L. M., *Angew. Chem. Int. Ed.*, **2016**, *55*(18), 5277

[17] Zhang Y. J., Wang Y. C., Jiang H. Q., Huang M. H., *Small*, **2020**, *16*(20), 2002550

[18] Zhao S. N., Li J. K., Wang R., Cai J. M., Zang S. Q., *Adv. Mater.*, **2022**, *34*(5), 2107291

[19] Zheng X. B., Yang J. R., Xu Z. F., Wang Q. S., Wu J. B., Zhang E. H., Dou S. X., Sun W. P., Wang D. S., Li Y. D., *Angew. Chem. Int. Ed.*, **2022**, Doi: org/10.1002/anie.202205946

[20] Li L., Chu M. Y., Song R. R., Liu S. H., Ren G. M., Xu Y., Wang L., Xu Q. F., Shao Q., Lu J. M., Huang X. Q., *Chem. Catal.*, **2022**, *2*(7), 1709

[21] Chauhan M., Reddy K. P., Gopinath C. S., Deka S., *ACS Catal.*, **2017**, *7*(9), 5871

[22] Yao N., Wang G. W., Jia H. N., Yin J. L., Cong H. J., Chen S. L., Luo W., *Angew. Chem. Int. Ed.*, **2022**, *61*(28), e202117178

[23] Huang W. Z., Li J. T., Liao X. B., Lu R. H., Ling C. H., Liu X., Meng J. S., Qu L. B., Lin M. T., Hong X. F., Zhou X. B., Liu S. L., Zhao Y., Zhou L., Mai L. Q., *Adv. Mater.*, **2022**, *34*(18), 2200270

[24] Li Q., Wang X. F., Tang K., Wang M. F., Wang C., Yan C. L., *ACS Nano*, **2017**, *11*(12), 12230

[25] Peng O., Shi R., Wang J., Zhang X., Miao J., Zhang L., Fu Y., Madhusudan P., Liu K., Amini A., Cheng C., *Mater. Today Energy*, **2020**, *18*, 100513

[26] Zhou X. Y., Gao J. J., Hu Y. X., Jin Z. Y., Hu K. L., Reddy K. M., Yuan Q. H., Lin X., Qiu H. J., *Nano Lett.*, **2022**, *22*(8), 3392

[27] Jin H. H., Zhao X., Liang L. H., Ji P. X., Liu B. S., Hu C. X., He D. P., Mu S. C., *Small*, **2021**, *17*(29), 2101001

[28] Mu X. Q., Yuan H. M., Jing H. Y., Xia F. J., Wu J. S., Gu X. Y., Chen C. Y., Bao J. C., Liu S. L., Mu S. C., *Appl. Catal. B: Environ.*, **2021**, *296*, 120095

[29] Yao Q., Huang B. L., Zhang N., Sun M. Z., Shao Q., Huang X. Q., *Angew. Chem. Int. Ed.*, **2019**, *58*(39), 13983

[30] Bai L. C., Hsu C. S., Alexander D. T. L., Chen H. M., Hu X. L., *J. Am. Chem. Soc.*, **2019**, *141*(36), 14190

[31] Xiao M. J., Zhang C. T., Wang P. Y., Zeng W. H., Zhu J. W., Li Y., Peng W., Liu Q., Xu H. W., Zhao Y. F., Li H. W., Chen L., Yu J., Mu S. C., *Mater. Today Phys.*, **2022**, *24*, 100684

[32] Feng C., Zhang Z. R., Wang D. D., Kong Y., Wei J., Wang R. Y., Ma P. Y., Li H. L., Geng Z. G., Zuo M., Bao J., Zhou S. M., Zeng J., *J. Am. Chem. Soc.*, **2022**, *144*(21), 9271

[33] Lee W. H., Han M. H., Ko Y. J., Min B. K., Chae K. H., Oh H.-S., *Nat. Commun.*, **2022,** *13*, 605

[34] Chen D. W., Dong C. L., Zou Y. Q., Su D., Huang Y. C., Tao L., Dou S., Shen S. H., Wang S. Y., *Nanoscale*, **2017**, *9*, 11969

[35] Zhang N., Hu Y., An L., Li Q. Y., Yin J., Li J. Y., Yang R., Lu M., Zhang S., Xi P. X., Yan C. H., *Angew. Chem. Int. Ed.* **2022**, *61*, e2022072